RSC Advances

ROYAL SOCIETY
OF **CHEMISTRY**

www.rsc.org/advances

Journal Name

Dynamic Article Links ▶

ARTICLE TYPE

Cross-linked multiblock copoly(arylene ether sulfone) ionomer/nano-ZrO₂ composite anion exchange membranes for alkaline fuel cells

Xiuhua Li,[*,a,b] **Jinxiong Tao,**[a,b] **Guanghui Nie,**[a,b] **Liuchan Wang,**[a,b] **Liuhong Li,**[a,b] **Shijun Liao**[a,b]

A series of cross-linked multiblock copoly(arylene ether sulfone) ionomer/nano-ZrO₂ (CLQCPAES/nano-ZrO₂) composite anion exchange membranes were prepared via block copolymerization, bromomethylation, ultrasonication blending, self-crosslinking, quaternization and alkalization. The structure and the surface and cross section morphology of the CLQCPAES/nano-ZrO₂ composite
10 membranes were characterized by solubility test, FT-IR, XRD and SEM analyses. The combination of the determining results reveals that the CLQCPAES/nano-ZrO₂ composite membranes are complex cross-linking networks of hydrophobic domains/hydrophilic domains/nano-ZrO₂ with clear zonal distribution of uniform nano-sized particles in the hydrophilic domains when the nano-filler loading below 7.5%. Basic performances of the CLQCPAES/nano-ZrO₂ composite membranes are assessed to investigate their
15 application in fuel cells in terms of water uptake, swelling ratio, ion exchange capacity (IEC), hydroxide conductivity, thermal and mechanical properties, and alkaline stability. The modification of anion exchange membranes with multiblock ionomer structure, cross-linking technique and the introduction of nano-ZrO₂ particles greatly enhance the water uptake, hydroxide conductivity, mechanical properties and alkaline stability of the composite membranes. Particularly, the CLQCPAES/7.5%ZrO₂ membrane with
20 an IEC value of 1.23 mmol g^{-1} exhibits the best comprehensive properties and constitutes a good potential candidate of anion exchange membrane used in AEMFCs.

1. Introduction

With the increase of energy crisis and environment problems, fuel cells have been regarded as one of the most promising energy
25 conversion devices that could provide clean and efficient energy for stationary and mobile applications, transportation, and portable power applications.[1-4] Recently, there is growing interest in anion exchange membrane fuel cells (AEMFCs) due to their several advantages over proton exchange membrane fuel cells,
30 including better electrode reaction kinetics, low fuel permeability, and the potential to use cheap transition metals such as Ag, Co or Ni as electro catalysts because of their low overpotentials associated with electrochemical reactions in alkaline conditions.[5-7] Moreover, more alternative fuels could be used in AEMFCs
35 owing to their low overpotential for hydrocarbon fuel oxidation and reduced fuel crossover, such as methanol, ethanol and ethylene glycol.[8-12] These fuels have several advantages like easier storage and transportation, and higher volumetric energy densities compared to hydrogen.
40 Anion exchange membranes (AEMs), key component serving as the electrolyte, play a key role in the performance of AEMFCs.

[a] School of Chemistry & Chemical Engineering, South China University of Technology, Guangzhou 510641, P. R. China.
45 *Fax: +86-20-2223-6591; Tel: +86-20-2223-6591;*
E-mail: lixiuhua@scut.edu.cn
[b] The Key Laboratory of Fuel Cell Technology of Guangdong Province, South China University of Technology, Guangzhou 510641, P. R. China.

The primary requirements of practical membranes for AEMFCs
50 include high ionic conductivity, good mechanical and thermal stability, and long-term alkaline stability. Unfortunately, the commercially available AEMs based on quaternary ammonium substituted cross-linked polystyrene are not suitable for AEMFCs due to their instability in alkaline condition.[13, 14] In order to
55 develop AEMs with good performance that could be used in alkaline fuel cells, many efforts have been devoted. A variety of polymeric AEMs have been synthesized and well explored, including poly(arylene ether)s,[15-23] partially fluorinated poly(arylene ether)s,[24-26] polybenzimidazole,[27] poly(ether
60 imide)s,[28] poly(phenylene oxide),[29] poly(vinyl alcohol),[30, 31] et al. In the case of polymeric AEMs, solving the balance problem between the membrane dimension stability and hydroxide ion conductivity must be taken into full consideration. In addition, to synthesize AEMs with well-designed structures safely is critical
65 for their large scale application. Currently, many new kinds of AEMs have been achieved by changing the chemistry of the polymers and functionalization techniques, as well as modifying the processing of the membranes. Block-polymer ionomers AEMs have demonstrated enhancing hydroxide conductivity,
70 mechanical and chemical stabilities due to improving phase separation between hydrophilic and hydrophobic domains.[19, 22, 23, 32, 33] However, the mechanical properties and chemical stability of this type of membranes strongly rely on the nature of the swollen hydrophilic domains. Overly high density of ammonium

groups in hydrophilic blocks can lead to excessive polymer swelling upon hydration and concomitant loss of mechanical properties.[22] The membranes with best comprehensive properties can be obtained with matched hydrophobic/hydrophilic block structures, such as QPAE-X15Y15 (X15 represents the hydrophobic blocks with a polymerization degree of 15, Y15 represents the hydrophilic precursor blocks with a polymerization degree of 15).[23] Moreover, the cross-linking techniques, including ionic crosslinking[31, 34-36] and covalent crosslinking,[20, 37, 38] have been proved to be practical methods to enhance the performance of AEMs. Na etc. reported the benzyl bromide groups can undergo covalent cross-linking reaction with aromatic rings belonging to the same or different polymer chains without adding catalyst or crosslinking reagent through a Friedel-Crafts mechanism and gave alkaline anion exchange membranes with enhanced alkaline stability and low fuel permeability.[39] This method is effective and easily controllable. Recently the organic-inorganic composite membranes with a combination of remarkable functionality of organic materials and high stability of inorganic fillers have been drawing increasing attention in fuel cells due to their high ionic conductivity and enhanced mechanical properties.[40] Up to now, several kinds of inorganic fillers have been used to modify the AEMs, such as α-Al_2O_3,[41] SiO_2,[42-44] Bentonite,[45] Mg-Al LDH,[46] TiO_2,[47-49] and ZrO_2.[50, 51] Among them, ZrO_2 is distinguished for its good surface hydrophilicity and chemical stability in acidic or alkaline environments. Especially, nano-sized ZrO_2 particles, which have large surface area and high activity, and good chemical and thermal stability, have been gaining much more attention in AEMs. In the previous work, we found that the introduction of nano-ZrO_2 can induce the crystallization of the matrix and enhance the IEC of the composite membranes due to the strong interaction between the ionomer and the filler particles. The QPAES/nano-ZrO_2 composite membranes show improved water uptake, hydroxide ion conductivity, mechanical properties, and thermal and chemical stabilities.[50]

Chloromethylation is the most widely-used method to introduce the cationic quaternary ammonium groups to the skeleton of polymers. However, this method has several drawbacks such as the strong toxicity of the commonly used chloromethylation reagent chloromethyl methyl ether, poor controllability of the chloromethylation position and quantity, and long reaction time.[15, 23, 52, 53] It has been proved that synthesizing polymeric ionomers by bromination of the precursor polymers containing benzylmethyl side groups is a much safer, faster (about 4h) and more controllable process and has drawn more attention recently.[18-21, 33, 39, 54]

In this work, we designed and synthesized a new multiblock copolymer with matching hydrophobic/hydrophilic block structure, which have four benzylmethyl side groups in the precursor of hydrophilic segments. We moderately brominated the precursor block polymer to control the density of ammonium groups, and dispersed various amounts of nano-ZrO_2 particles into the brominated polymer to get nano-ZrO_2 composite membranes. By controlling the heat treatment condition of the preparation process of the membranes, we introduced cross-linked structure into nano-ZrO_2 composite membranes. The ultimate objective of this paper is to produce and evaluate nano-

ZrO_2 composite AEMs with block and cross-linking structures. The procedure was given careful consideration to the selective ionizations at specific segments, reinforcing effect of nano-ZrO_2 particles, and the combination of the positive functions of block and cross-linking structures. The structure of the obtained quaternized composite membranes is confirmed by FT-IR, X-ray diffraction (XRD), scanning electron microscopy (SEM). Water uptake, swelling ratio, hydroxide ion conductivity, and mechanical properties of the membranes are investigated, as well as their thermal and chemical stability.

2. Experimental Section

2.1 Materials

Bis(4-fluorophenyl) sulfone (FPS), Nano-zirconia filler (nano-ZrO_2) and 3,3',5,5'-tetramethyl-4,4'-dihydroxybiphenyl (TMBP) were purchased from Aladdin Reagent, Shanghai, China. Bis(4-hydroxylphenyl)diphenyl methane (HPDPM) were synthesized according to Wang's work.[55] 1,1,2,2-tetrachloroethane, N-bromosuccinimide (NBS), azodiisobutyronitrile (AIBN), trimethylamine aqueous solution (33wt%), potassium carbonate, sodium hydroxide, toluene, methanol, and chloroform were obtained from commercial sources and used as received. N,N′-dimethylacetamide (DMAc) and N,N′-dimethylformamide (DMF) were dried over 4 Å molecular sieves. Toluene was dried over sodium wire prior to use.

2.2 Synthesis of precursor bromomethylated multiblock copoly(arylene ether sulfone) (BMCPAES)

A hydroxyl-terminated hydrophilic oligomer of X12 and a fluorine-terminated hydrophobic oligomer of Y10 (numbers after X and Y represent the polymerization degrees of the hydrophilic/hydrophobic oligomers) were synthesized via polycondensation of TMBP with FPS, and HPDPM with FPS with controlled feed ratios following a similar procedure in the previous work.[23] A multiblock copolymer containing benzylmethyl groups (MCPAES) was synthesized via copolycondensation with an equimolar amount of X12 and Y10. A solution of 5 wt% MCPAES in 1,1,2,2-tetrachloroethane underwent the bromination with NBS (molar ratio of NBS to methyl group = 2.7:1) and AIBN (5 mol% of NBS) at 80 °C for 4 h. The bromomethylated multiblock copolymer BMCPAES with 1.87 benzylmethyl bromide groups per repeating unit of the hydrophilic blocks and Mn = 65800 Da was received via free radical substitution reaction. The yield is 91.7%.

2.3 Preparation of cross-linked multiblock copoly(arylene ether sulfone) ionomer/nano-ZrO_2 (CLQCPAES/nano-ZrO_2) composite membranes

1.5 g of BMCPAES dissolved in 11 mL of 1,1,2,2-tetrachloroethane. 0.038 g of nano-sized ZrO_2 was added in 4 mL of 1,1,2,2-tetrachloroethane and subjected to ultrasonication for about 0.5 h. Then the mixture was mixed with the solution of BMCPAES and treated under ultrasonication for another 1 h. The final mixture was cast into a composite membrane on a clean glass plate. The membrane was dried at 60 °C for 24 h in order to remove the solvent thoroughly. The obtained composite membrane was treated at 130 °C for 3 h in a vacuum oven to give a cross-linked membrane. The membrane was quaternized with a

33 wt % trimethylamine solution according to the same conditions as in the previous work.[23] After that the membrane underwent the ion exchange reaction with a 1 M NaOH solution at room temperature for 48 h to convert the counter anion from bromine to hydroxide anion and give a cross-linked quaternized membrane CLQCPAES/2.5%ZrO₂. The others CLQCPAES/nano-ZrO₂ composite membranes with 5, 7.5 and 10 wt % of nano-ZrO₂ were prepared following the similar procedure of CLQCPAES/2.5%ZrO₂. QCPAES and CLQCPAES membranes were prepared by the procedures without the addition of nano-ZrO₂ and/or heat crosslinking respectively to make comparison. These membranes were washed thoroughly and soaked in deionized water prior to analysis.

2.4 Membrane characterization

2.4.1 The weight residual of the brominated cross-linked membranes

The weight residual of the brominated cross-linked composite membranes after dissolving in good solvents for the original polymers is a directive parameter for the degree of the cross-linking reactions. The composite membranes were immersed in DMF at ambient temperature for 24 h. Then the solvent was removed and the residual samples were collected, washed, dried, and weighed. The weight residuals (W_R) of the cross-linked membranes were calculated with the equation:

$$W_R = \frac{W_A}{W_F} \times 100\%$$

where W_A is the weight of the cross-linked membranes after being immersed in DMF, and W_F is the former weight of the cross-linked membranes.

2.4.2 Structure, morphology, thermal analysis and mechanical properties

Fourier transform infrared (FT-IR) spectra were recorded on a Bruker Tensor 27 instrument. The X-ray diffraction measurements were performed to examine the crystallinity of the composites membranes by an X-ray diffractometer (PANALYTICAL, Holland). Scanning electron microscope (SEM) surface images were taken using a NOVA NANOSEM 430 with an accelerating voltage of 10 kV to investigate the composite membrane morphologies. Thermogravimetric analysis (TGA) was performed under nitrogen atmosphere using a TAINC SDT Q600 thermogravimetric analyzer at a heating rate of 10 °C per minute from 35 to 700 °C. The tensile properties of membranes were measured by using an Instron M3300 at 25 °C and 100% RH at a stretching speed of 10 mm min⁻¹.
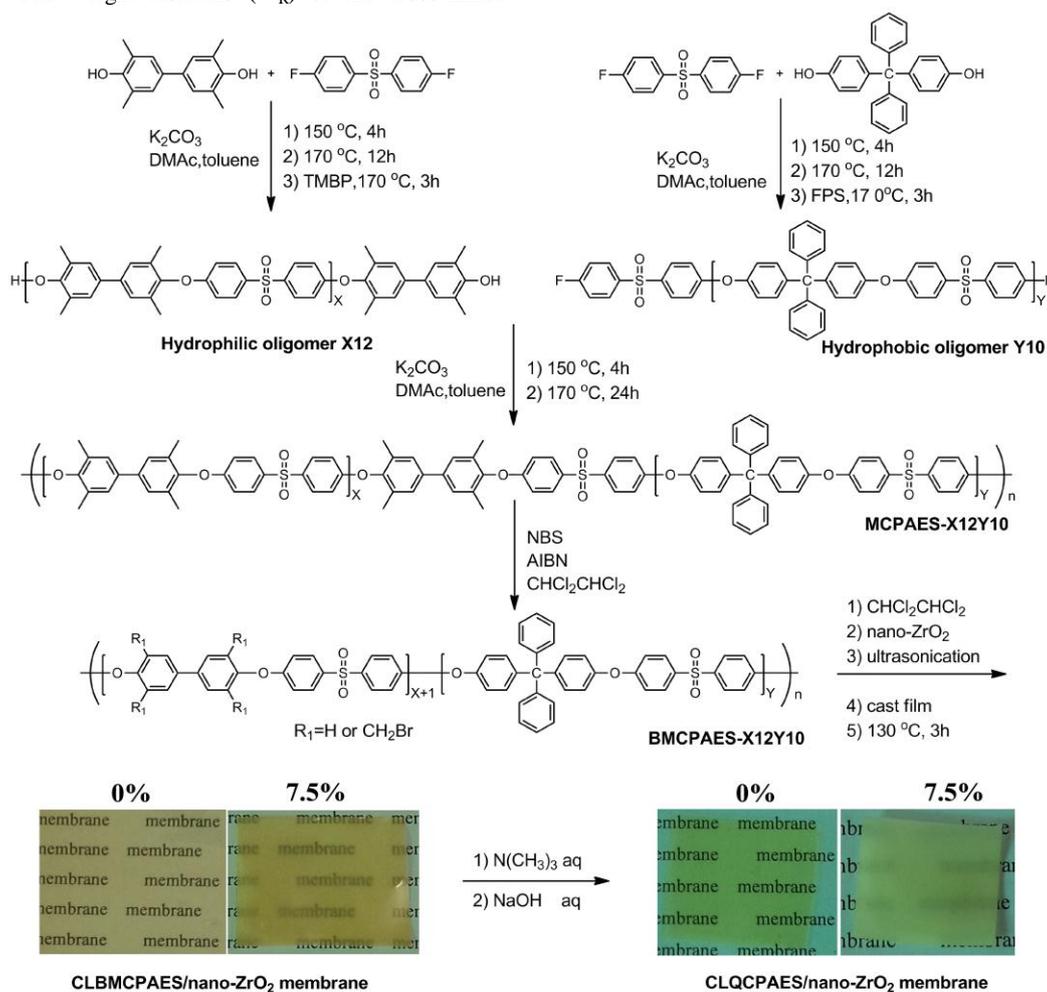
Scheme 1 Fabrication route of the CLQCPAES/nano-ZrO₂ composite AEMs

2.4.3 Ion exchange capacity, water uptake, swelling ratio and hydroxide ion conductivity

We assessed the basic properties of the CLQCPAES/Nano-ZrO$_2$ composite membranes in terms of ion exchange capacity, water uptake, swelling ratio and hydroxide conductivity following the same methods as that in the previous work.[16]

The ion exchange capacities (IECs) of the CLQCPAES/nano-ZrO$_2$ composite membranes and original ionomer membranes were measured using back-titration. The IEC values were obtained using the expression:

$$IEC = \frac{V_{HCl}C_{HCl} - V_{NaOH}C_{NaOH}}{m_{dry} - (V_{HCl}C_{HCl} - V_{NaOH}C_{NaOH})(M_{Cl^-} - M_{OH^-})}$$

where V_{HCl} (mL) and C_{HCl} (M) are the volume and concentration of the initial solution of standardized HCl. V_{NaOH} (mL) and C_{NaOH} (M) are the volume and concentration of the standardized NaOH solution used in back titration. m_{dry} is the weight of the dried sample after treated in vacuum at 80 °C for 24 h. M_{Cl^-} and M_{OH^-} are the molar mass of Cl$^-$ and OH$^-$ groups respectively.

The water uptakes and swelling ratios of the CLQCPAES/Nano-ZrO$_2$ composite membranes were determined with the strip samples (5 cm in length and 0.7 cm in width). The values of water uptakes and swelling ratios were calculated with the following equations respectively:

$$WU = \frac{W_{wet} - W_{dry}}{W_{dry}} \times 100\%$$

$$SR = \frac{L_{wet} - L_{dry}}{L_{dry}} \times 100\%$$

where W_{wet} is the weight for the wet sample and W_{dry} is the weight of the dried sample after drying to a constant under vacuum at 80 °C. L_{wet} and L_{dry} are the lengths of the wet and dry membrane sample.

The through plane hydroxide ion conductivity measurements of the CLQCPAES/Nano-ZrO$_2$ composite membranes were taken with an IviumStat frequency response analyzer using a two probe method at an oscillating voltage of 10 mV, and the frequency ranging from 1 KHz to 1 MHz The conductivity was calculated using the following equation:

$$\sigma = \frac{L}{RA}$$

where L (cm) and R (Ω) are the thickness and resistance of the membrane, A (cm^2) is the electrode area.

2.4.4 Alkaline stability

We evaluated the stability of the CLQCPAES/Nano-ZrO$_2$ composite membranes in alkaline environments by three methods. The first one was used to assess short term stability under a cruel alkaline circumstance of 6 M NaOH solution. The hydroxide ion conductivity of the treated membranes was measured after immersing in 6 M NaOH solution at room temperature for 48 h. The other two methods aimed at evaluating the long-term chemical stability of the membranes. In the case of the second method, the membrane samples were kept in 6 M NaOH solution at 60 °C and shaken slightly every 12 h to see when they broke into pieces. In the case of the third method, the membrane samples were immersed in 1 M NaOH solution at 60 °C for 340 h and the hydroxide ion conductivity of the treated samples was measured at 60 °C.

3. Results and Discussion

3.1 Fabrication, structure characteristic and morphology of the CLQCPAES/nano-ZrO$_2$ composite membranes
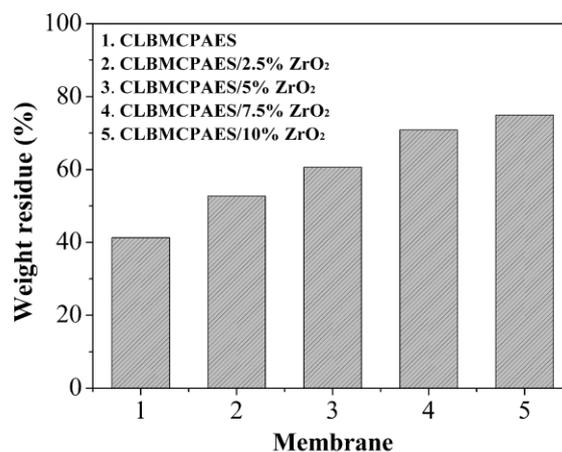
Fig. 1 Weight residuals of the CLBMCPAES/nano-ZrO$_2$ composite membranes after immersing in DMF at room temperature for 24 h.

The fabrication route of the cross-linked multiblock ionomer/nano-ZrO$_2$ composite anion exchange membranes (CLQCPAES/nano-ZrO$_2$ composite AEMs) is shown in scheme 1. The hydroxyl-terminated hydrophilic oligomer X12 and fluorine-terminated hydrophobic oligomer Y10 were synthesized by controlling the molar ratio of monomers. The average oligomers lengths, which were calculated from the ^{1}H NMR data (Fig. S1 & S2) according the previous work,[23] agree well with the designed oligomers sizes. The multiblock copolymer MCPAES was synthesized via copolycondensation of an equimolar amount of the two oligomers. The bromomethylated multiblock copolymer BMCPAES with 1.87 benzylmethyl bromide groups per repeating unit of the hydrophilic blocks (Fig. S3) and Mn of 65800 Da was obtained via a free radical substitution reaction using NBS as bromine agent and AIBN as initiating agent. The uncrosslinked composite membranes were prepared via the ultrasonic blending method. In the previous work, we found that the agglomeration of the nano-ZrO$_2$ particles restricts the modification of nano-fillers to the composite AEMs.[50] In this work we firstly dispersed the agglomerated particles of nano-ZrO$_2$ filler in 4 mL of 1,1,2,2-tetrachloroethane under ultrasonic treatment to separate the fillers into nano-sized particles. Then the mixture was added to the pre-made BMCPAES solution for further ultrasonic blending. Due to the drag force of viscous-fluid, the nano-sized particles can't agglomerate into large particles and form well distribution of nano-sized filler particles in the casting mixture. According to Na's work, the benzylmethyl bromide groups could react with electron-rich aromatic rings via Fridel-Crafts mechanism at high temperature.[39] Fig.1 shows the weight residuals of the cross-

linked composite BMCPAES/nano-ZrO$_2$ membranes after immersing in DMF under intense stirring at room temperature for 24 h. DMF is a very good solvent for the original multiblock polymer BMCPAES. After undergoing the cross-linking reaction

5 at 130 °C, the polymeric matrix becomes partially insoluble in DMF. This is a strong proof of successful introduction of cross-linked structure into the matrix. The weight residuals of the CLBMCPAES/nano-ZrO$_2$ composite membranes increase with the increase of nano-filler loading. The weight residuals greatly

10 excesses the sum of the filler loading and the calculated gel content of the matrix. It is obvious that the nano-ZrO$_2$ particles are active under the environment of cross-linking and the surface hydroxyl groups can react with the benzylmethyl bromide groups of the polymeric matrix. Combined with the conductions that the

15 hydroxide ions associated with quaternary ammonium groups can form interfacial hydrogen bonds with the surface hydroxyl groups of nano-ZrO$_2$ filler particles and strong interactions with the others quaternary ammonium cations inside the ionic polymer matrix, which is based on the random ionomer/nano-ZrO$_2$

20 composite AEMs,[50] we depicted the structure of the cross-linked multiblock composite AEMs as shown Fig. 2. The membranes were then treated by quaternization and alkalization.
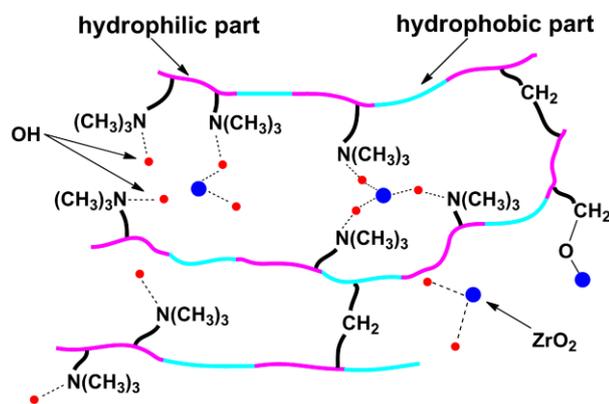
Fig. 2 Schematic diagram of the structure of the CLQCPAES/
25 nano-ZrO$_2$ composite AEMs.

The chemical structures of the CLQCPAES/nano-ZrO$_2$ composites AEMs were characterized by FT-IR. Fig. 3 shows the FT-IR spectra of BMCPAES, CLBMCPAES,
30 CLBMCPAES/7.5%ZrO$_2$ and CLQCPAES/7.5%ZrO$_2$. In Fig. 3(**a**), the absorption signals ranging from 3095 to 2987 cm^{-1} are attributed to the aromatic C-H stretching vibration, and those signals at 2924 and 2860 cm^{-1} are assigned to aliphatic C-H bonds of methylene and methyl groups respectively. The signals
35 at 1590 and 1495 cm^{-1} are characteristic absorption peaks of the C=C skeletal vibrations of aromatic rings. The sharp and strong signals at 1295 and 1146 cm^{-1} are contributed to the asymmetric and symmetric stretching vibrations of O=S=O bonds. The wide signal around 1250 cm^{-1} is attributed to the stretching vibrations
40 of Ar-O-Ar. The signal at 874 cm^{-1} is assigned to the bending vibrations of the isolated Ar-H in the tetra-substituted aromatic rings. The signal at 846 cm^{-1}is assigned to the bending vibrations of the continuous Ar-Hs in the para-substituted aromatic rings
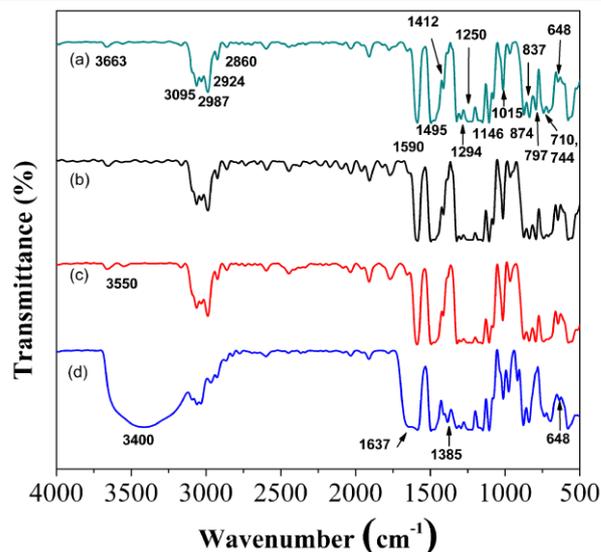
Fig. 3 FT-IR spectra of (a) BMCPAES, (b) CLBMCPAES, (c)
45 CLBMCPAES/7.5%ZrO$_2$, and (d) CLQCPAES/7.5%ZrO$_2$.

containing O=S=O group. The signal at 797 cm^{-1} is assigned to the bending vibrations of the continuous Ar-Hs in the para-substituted aromatic rings in the moieties of tetra-phenyl methyl
50 group. The signals at 744 and 710 cm^{-1} are characteristic absorptions of the bending vibrations of the continuous Ar-Hs in the mono-substituted aromatic rings in the moieties of tetra-phenyl methyl group. These signals are the characteristic absorption bands of the polymer matrix backbone and can be
55 observed clearly in the FT-IR spectra of all kinds of the membranes. A decrease of the signal at 710 cm^{-1} and an increase of the signal at 797 cm^{-1} are observed simultaneously in the FT-IR spectrum of CLBMCPAES (Fig. 3(**b**)). These are the direct proofs for the cross-linking positions at the pendent mono-
60 substitute benzene rings in the moieties of tetra-phenyl methyl group. A new weak signal at 3350 cm^{-1} appears in the FT-IR spectrum of CLBMCPAES/7.5%ZrO$_2$ (Fig. 3(**c**)), which is assigned to the characteristic absorption of the surface hydroxide groups of nano-ZrO$_2$ particles because of the hygroscopicity of
65 nano-ZrO$_2$ particles and good isolation of the nano-filler. Compared with the spectra of CLBMCPAES and CLBMCPAES/7.5%ZrO$_2$ (Fig. 3(**b-c**)), the characteristic signals for hydroxide groups change into a strong wide peak ranging from 3700 to 3100 cm^{-1} owing to the strong hydrophilicity of the
70 quaternary ammonium hydroxide and strong hydrogen bonds between the hydroxide groups and absorbed water molecules in the spectrum of CLQCPAES/7.5%ZrO$_2$ (Fig. 3(**d**)). The new signal at 1380 cm^{-1} is attributed to methyl group of the quaternary ammonium groups. The signal at 1635 cm^{-1} originating from the
75 Zr−O−Zr is widen and enhanced by the strong hydrogen bond from the absorbed water molecules. This signal in the spectrum of CLBMCPAES/7.5%ZrO$_2$ is totally covered with the C=C skeletal vibrations of 1590 cm^{-1}. The characteristic absorption signal of C-Br at 648 cm^{-1} still remains in Fig. 3(**d**) reveals the
80 incomplete quaternization of the CLQCPAES/7.5%ZrO$_2$ composite membrane.
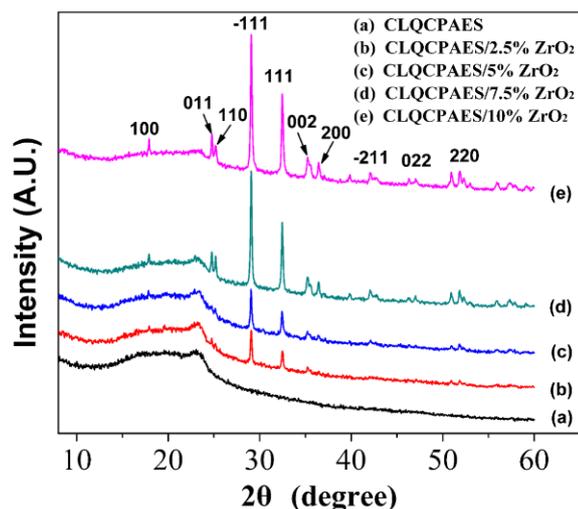
Fig. 4 XRD patterns of CLQCPAES membrane and CLQCPAES/nano-ZrO_2 composite membranes: (a) CLQCPAES, (b) CLQCPAES/2.5%ZrO_2, (c) CLQCPAES/5.0%ZrO_2, (d) CLQCPAES/7.5% ZrO_2, and (e) CLQCPAES/10% ZrO_2.

The X-ray diffraction measurements were further used to determine the crystallinity of the CLQCPAES and CLQCPAES/nano-ZrO_2 composite membranes. Fig. 4 illustrates the diffraction pattern of the membranes. The crystallinity of the membranes, which is calculated by JADE 7.0, is listed in Table 1. As can be seen in Fig. 4(**a**), only a halo at $2\theta = 13-40^o$ is found in the diffractogram of CLQCPAES. This indicates that the polymeric matrix is totally amorphous. Several sharp and intense signals appear in the patterns of composite membranes (Figure 4(**b-e**)), which are assigned to (100), (011), (110), (-111), (111), (002), (200), (021), (-211), (022) and (220) facets of ZrO_2 respectively according to the standard diffractogram of ZrO_2. The crystallinity of composite membranes increases with the increasing nano-filler loading and is lower than their content of nano-ZrO_2 when the filler concentration is below 7.5% (Table 1). An enhancement of crystallinity of composite membrane is observed with CLQCPAES/10%ZrO_2 membrane. This agrees well with the results of the previous work about the random ionomer/nano-ZrO_2 composite membranes.[50] The difference in the enhancement of crystallinity of the composite membranes may reside in the well dispersion of nano-filler in CLQCPAES/nano-ZrO_2 AEMs with nano-particles' size below 300 nm (Fig. 5) and the agglomerating particles of 1000-2000 nm in the random ionomer/nano-ZrO_2 composites membranes [50]. The small size of the nano fillers weakens the nucleating effect of nano-ZrO_2 particles. Another reason is that the positions of ammonium groups in these two kinds of ionomer are different. The ammonium groups in CLQCPAES locate at the main chain skeleton of the hydrophilic blocks. The ammonium groups in random ionomer locate both at the main chain skeleton and pendant phenyl rings of tetraphenyl methyl moieties.

SEM photographs of the pure CLQCPAES and CLQCPAES/nano-ZrO_2 AEMs, which are shown in Fig. 5 and Fig. S4, were taken to examine the surface and cross section morphology. The SEM surface section photograph of the pure CLQCPAES membrane (Fig. 5(**a**)) shows a smooth, uniform and dense morphology. As to the composite membranes (Fig. 5(**b-e**)), we can see that the ZrO_2 particles are well dispersed and there is no obvious agglomerates of nano-ZrO_2 in the composite membranes even when the nano-filler loading is up to 10% (Fig. 5(**e**)). The dispersion of nano-filler particles in this work is much better than that of the nano-fillers in the reported composite membranes.[48, 50, 51] The result reveals that the modified ultrasonication blending method used in this work is effective to prepare organic-inorganic hybrid membranes. In the case of CLQCPAES/nano-ZrO_2 AEMs, we can observe clear zonal distribution of uniform nano-sized particles when the nano-filler loading is below 7.5%. The reasonable explanation is the strong coordination between hydrophilic domains and the nano-ZrO_2 particles and relatively poor interaction between the hydrophobic domains and the nano-filler particles. The clear zonal distribution turns vague and uniform distribution of nano-filler particles is observed in the image of CLQCPAES/10%ZrO_2 (Fig. 5(**e**)). Moreover the average size of nano-ZrO_2 particles in CLQCPAES/10%ZrO_2 is larger than that of others CLQCPAES/nano-ZrO_2 AEMs due to excess addition of nano-fillers. The dispersion of nano-filler particles in the SEM cross section images of the AEMs (Fig. S4) strongly support the conclusions from the surface section photographs. It should be noted that there is no obvious interface between the matrix and the nano-filler particles. This confirms again the existence of the strong chemical and physical interactions between them.

3.2 Ion exchange capacity (IEC), water uptake (WU), swelling ratio (SR) and hydroxide conductivity

The IEC value reflects the number of functional groups in the polymer, and determines the transport capacity of AEMs for hydroxide ion. Table 1 lists the IEC values of QCPAES, CLQCPAES and the composite membranes based on CLQCPAES. The IEC value of CLQCPAES shows a decrease of 0.19 meq g^{-1} compared with that of QCPAES, which is about 15.2% of the IEC value of QCPAES. This result isn't beyond expectation because the consumption of bromomethyl groups in the self-crosslinking process result in an decrease of bromomethyl groups to be quaternized in the polymeric matrix. The experimental IEC values of the CLQCPAES/nano-ZrO_2 composite membranes are much higher than the original IEC values calculated from IEC of the matrix CLQCPAES and the compositions of the composite membranes. The enhancement effect of the nano-sized ZrO_2 particles on the IEC values of the randon ionomer composite membranes has been reported.[50] In that case the nano-sized ZrO_2 particles evenly ditribute in the polymer matrix. In this work, the mutilblock ionomer endows clear zonal distribution of uniform nano-sized particles in the hydrophilic domains. This is bound to change the enhancement effection of the IEC values of the mutilblock ionomer based composite membranes. Moreover, the contribution ability of one percent of nano filler in the CLQCPAES/nano-ZrO_2 composite membranes to IEC values is closely controlled by the nano-filler loadings. The contribution ability of one percent of nano filler is calculated and shown in Table 1 as the parameter IEC of 1% ZrO_2. The contribution ability shows a decreasing trend with the increasing content of nano-ZrO_2. The contribution ability of nano-filler to IEC values in CLQCPAES/nano-ZrO_2 AEMs are
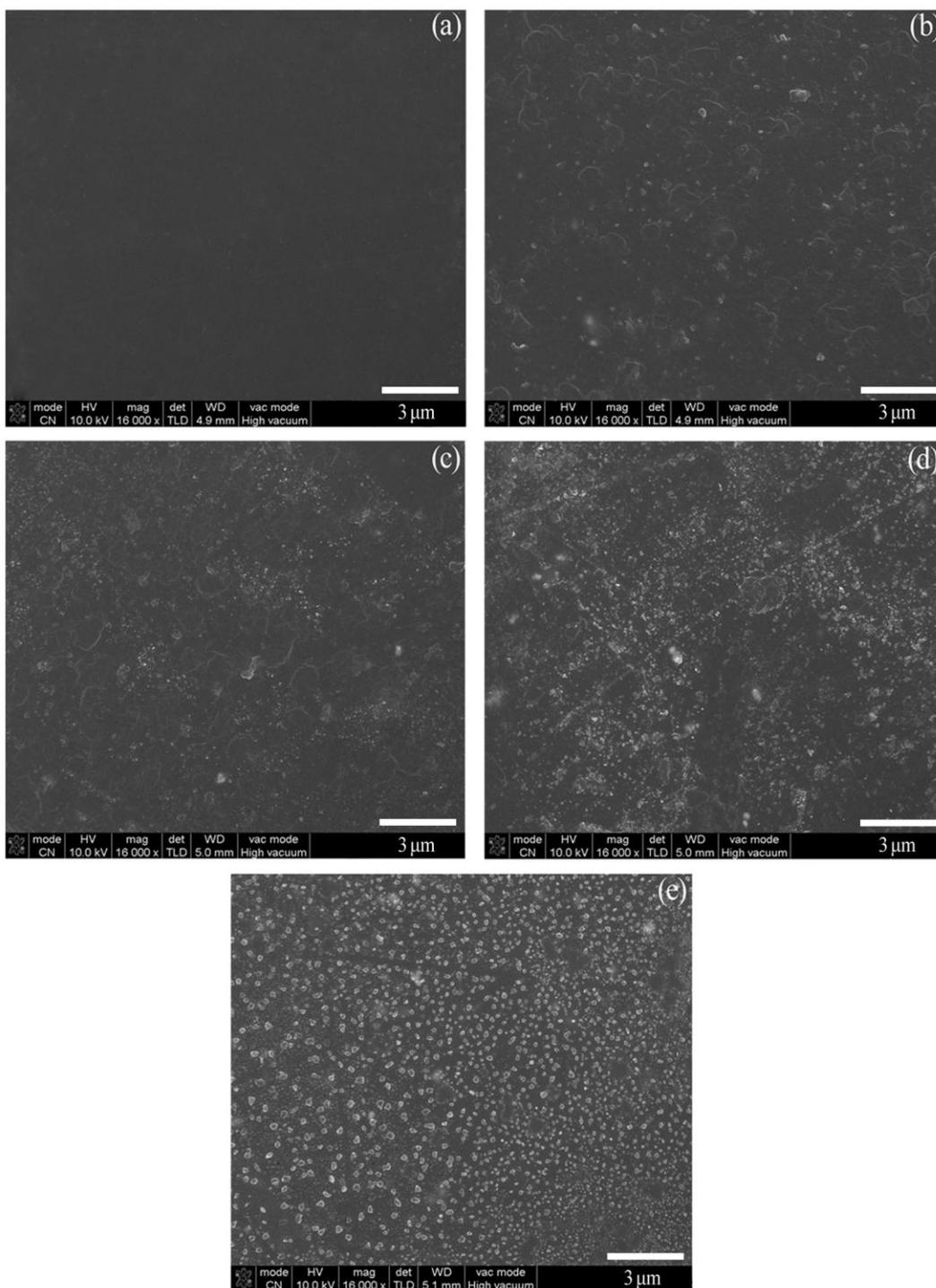
Fig. 5 SEM surface section images of CLQCPAES and CLQCPAES/nano-ZrO$_2$ composite membranes: (a) CLQCPAES, (b) CLQCPAES/2.5%ZrO$_2$, (c) CLQCPAES/5%ZrO$_2$, (d) CLQCPAES/7.5%ZrO$_2$, and (e) CLQCPAES/10%ZrO$_2$.

obviously lower than that of QPAE/nano-ZrO$_2$ AEMs.[50] The possible reasons are that the strong hydrophobic domains and the lower density of quaternary ammonium groups in the hydrophilic domains limit the coordination between the nano-ZrO$_2$ and hydroxide ions. The cumulative enhancement of the nano-ZrO$_2$ fillers displays the tendency that the values of IEC of the composite membranes increase with the increasing loading of nano-filler until the loading content is up to 7.5%. The IEC value

of CLQCPAES/10%ZrO$_2$ membrane shifts down because of the decreased active surface area of the nano-ZrO$_2$ particles resulting from the increasing size of nano-filler particles (Fig. 5(**e**)).

Water uptake and swelling ratio are two close paprameters playing key roles in hydroxide conductivity and mechanical properties of AEMs. The water uptakes and swelling ratios of CLQCPAES/nano-ZrO$_2$ composite membranes are listed in Table 2 and shown in Fig. 6 and Fig. 7. As can be seen, the water

Table 1 Values of crystallinity and IEC of QCPAES, CLQPCAES and CLQCPAES/nano-ZrO$_2$ composite membranes.

membrane	Crystallinity (%)	IEC[a] (meq g^{-1})	IEC[b] (meq g^{-1})	IEC of ZrO$_2$ (meq g^{-1})	IEC of 1% ZrO$_2$
QCPAES	0	-	1.25±0.09	0	0
CLQCPAES	0	1.06	1.06±0.03	0	0
CLQCPAES/2.5%ZrO$_2$	2.0	1.03	1.12±0.04	0.09	0.036
CLQCPAES/5%ZrO$_2$	2.8	1.00	1.15±0.06	0.15	0.030
CLQCPAES/7.5%ZrO$_2$	7.3	0.98	1.23±0.08	0.25	0.033
CLQCPAES/10%ZrO$_2$	10.9	0.95	1.18±0.06	0.23	0.023

[a] Calculated from IEC of the matrix and the compositions of the composite membranes.
[b] Determined by titration

Table 2 Water uptake, swelling ratio, and hydroxide conductivity of the QCPAES, CLQCPAES, and CLQCPAES/nano-ZrO$_2$ composite membranes.

membrane	IEC (meq g^{-1})	water uptake（%）		swelling ratio（%）		Conductivity（mS cm^{-1}）	
		20 ºC	80 ºC	20 ºC	80 ºC	20 ºC	80 ºC
QCPAES	1.25±0.09	59.8±2.6	63.0±3.1	15.3±0.7	18.0±1.1	16.2±0.3	50.6±0.4 (38.6, 60 ºC)
CLQCPAES	1.06±0.03	34.2±1.7	38.2±2.3	10.2±0.1	10.8±0.1	13.5±0.1	34.6±0.3 (27.4, 60 ºC)
CLQCPAES/2.5%ZrO$_2$	1.12±0.04	41.0±2.0	46.6±1.8	11.5±0.4	14.5±0.3	11.3±1.2	37.3±0.4
CLQCPAES/5%ZrO$_2$	1.15±0.06	48.6±1.4	57.0±3.2	13.6±1.0	15.6±0.7	9.8±0.5	42.7±0.2
CLQCPAES/7.5%ZrO$_2$	1.23±0.08	56.2±2.3	66.2±2.5	15.4±1.6	17.9±1.9	16.2±0.4	55.2±0.6
CLQCPAES/10%ZrO$_2$	1.18±0.06	52.0±0.8	55.9±1.9	11.5±0.8	15.1±1.3	14.9±0.4	49.4±0.7
QPAE-X25Y21[23]	1.15±0.13	14	24	7.6	15.4	15.0±0.7	33.7±0.2 (60 ºC)
QPAES/7.5%nano-ZrO$_2$[50]	1.74±0.03	23.8	52.7	not reported	8.6 (60 ºC)	19.8±0.8	41.4
PEEK-Q-80[20]	1.23	28.9	33.2	13.8	18.8	15	37
QMPAEK-70[54]	1.22	49.66 (RT)	69.19	8.39 (RT)	14.65	9.6 (RT)	24.1

uptakes and swelling ratios of cross-linked membranes are smaller than that of the uncross-linked multiblock ionomer membrane QCPAES. Especailly, the CLQCPAES membrane shows a swelling ratio of approximately 60 percent of that of QCPAES membrane. It is obvious that the enhancement of membrane dimenstability by the crosslinking technique is very effective. In the case of CLQCPAES/nano-ZrO$_2$ composite membranes, the water uptakes and swelling ratios increase with the increasing loading of nano-filler. The swelling ratios of crosslinked multiblock ionomer/nano-ZrO$_2$ composite membranes are bigger than that of the matrix CLQCPAES. This is reverse to that of the random ionomer/nano-ZrO$_2$ composite membranes.[50] The possible explanations are zonal distribution of uniform nano-sized particles in the hydrophilic domains and the integral effect of bonding water molecules from the continuous and strong hydrophilic quaternary ammonium groups in the hydrophilic blocks and the fixed hygroscopic nano-particles in the hydrophilic domains of CLQCPAES/nano-ZrO$_2$ composites membranes. Fig. 6 and Fig. 7 demonstrate the temperture dependences of water uptake and swelling ratio of the CLQCPAES/nano-ZrO$_2$ composite membranes and pure polymeric matrix membranes. All the membranes show a similar tendency that the water uptakes slowly increase with the increasing of temperature.

The hydroxide conductivity is one of the most important parameters of AEMs and strongly affects their fuel cell performance. The through plane hydroxide conductivities of QCPAES, CLQCPAES, and CLQCPAES/nano-ZrO$_2$ composite membranes at varying temperatureare are shown in Table 2 and Fig. 8. For convenience of comparision, the values of hydroxide conductivity (through plane) of the multiblock ionomer QPAE-X25Y21 with a closing IEC to that of QCPAES and CLQCPAES, which has a similar backbone to that of QCPAES, are also listed in Table 2. It is clear that the mutiblock configurations show a similar conductive behaviour taking account of small differences in IEC values and the crosslinking doesn't change the performance of conductive channels. What has been changed in CLQCPAES is the stereo distribution of the conductive channels.
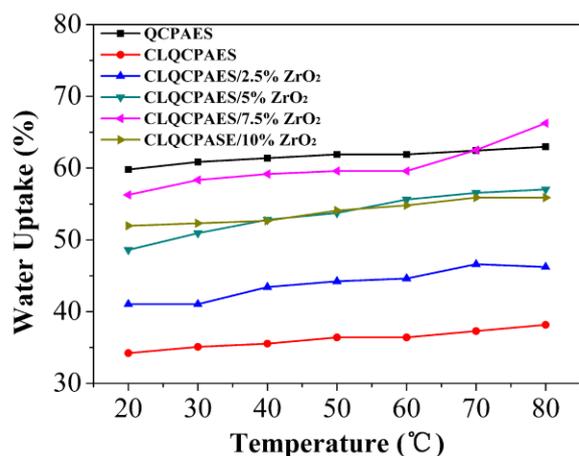
Fig. 6 Water uptakes of QCPAES, CLQCPAES and CLQCPAES/nano-ZrO$_2$ composite membranes at different temperature.
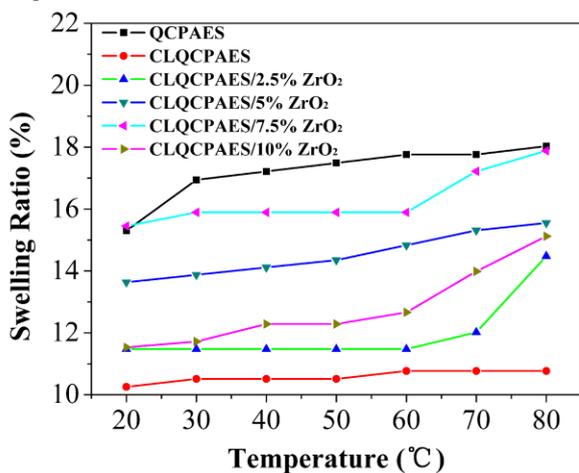
5 **Fig. 7** Swelling ratios of QCPAES, CLQCPAES and CLQCPAES/nano-ZrO$_2$ composite membranes at different temperature.
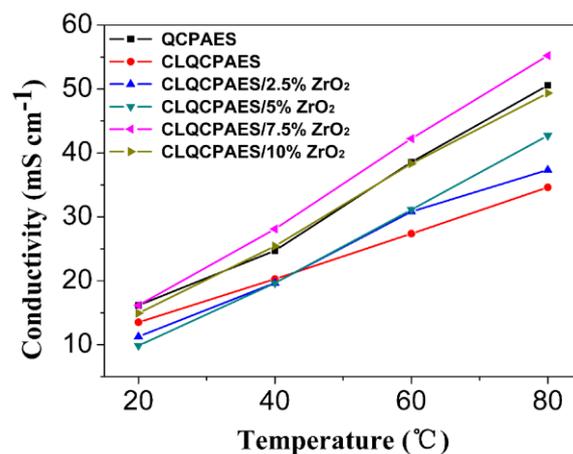
10 The modification of CLQCPAES with nano-ZrO$_2$ filler displays obvious enhancement of hydroxide conductivity at higher filler loading and/or higher temperature till the filler loadings are up to 7.5%. The CLQCPAES/7.5%ZrO$_2$ (1.23±0.08 meq g^{-1}) membrane shows the highest conductivity of 16.2 mS cm^{-1} at 20
15 °C and 55.2 mS cm^{-1} at 80 °C, respectively, and is obvious higher than that of radom ionomer composite membrane QPAES/7.5%ZrO$_2$ with a much higher IEC of 1.74±0.03 meq g^{-1},[50] and some reported AEMs with similar IEC.[20, 54] The reason is that the integral effect of bonding water from the dense and
20 strong hydrophilic quaternary ammonium groups and the fixed hygroscopic nano-particles in the hydrophilic domains of the CLQCPAES/nano-ZrO$_2$ composite membranes offers adequate water molecules inside the conductive channels and accelerates the surface site hopping and directional movement of hydroxide
25 ions. This kind of positive contribution to the membrane conductivity greatly countervails the conductivity loss resulting from the low IECs of the CLQCPAES/nano-ZrO$_2$ composite membranes. The enhancents of water uptake and IEC are weakened by the aggregation of nano-filler particles in the case of
30 CLQCPAES/10.0%ZrO$_2$ membrane (1.18±0.06 meq g^{-1}) (Table 1-2, Fig. 5(e)). The CLQCPAES membrane without addition of nano-ZrO$_2$ shows the lowest hydroxide conductivity of 13.5 mS cm^{-1} at 20 °C and 34.6 mS cm^{-1} at 80 °C owing to the lowest IEC

35 **Fig. 8** Hydroxide conductivity of QCPAES, CLQCPAES, and CLQCPAES/nano-ZrO$_2$ composite membranes at different temperature.

Fig. 9 Arrhenius plots of QCPAES, CLQCPAES and CLQCPAES/nano-ZrO$_2$ composite membranes: (a) QCPAES, (b)
40 CLQCPAES, (c) CLQCPAES/2.5%ZrO$_2$, (d) CLQCPAES/5%ZrO$_2$, (e) CLQCPAES/7.5%ZrO$_2$, and (f) CLQCPAES/10%ZrO$_2$.

among the cross-linking multiblock ionomer based membranes
45 and absence of the modification of nano-filler. For potential application in AEMFCs, there is a basic requirement for the membrane materials that hydroxide conductivity must be above 10 mS cm^{-1}.[56] Apparently all the composite membranes in this work fulfill this requirement and the CLQCPAES/7.5%ZrO$_2$
50 (1.23±0.08 meq g^{-1}) membrane is the best candidate. The differences in the temperature dependence of hydroxide conductivities of the composite membranes, which follows the Arrhenius behavior, can be explained by their inherent ion transport activation energies (E_a). The E_a value is calculated with
55 the equation: $E_a = -b \times R$. b is the slope of linear aggression of ln σ and 1000/T (where σ is the hydroxide conductivity and T is the absolute temperature), which follows Arrhenius behavior. E_a values of QCPAES, CLQCPAES and CLQCPAES/nano-ZrO$_2$ composite membranes are shown in Fig. 9. The E_a values of the
60 CLQCPAES/nano-ZrO$_2$ composite AEMs range from 17.28 to 21.26 kJ mol^{-1}, which are obviously higher than that of CLQCPAES membrane and close to that of multiblock ionomer membrane QCPAES. This enlightens us that the structures of the CLQCPAES/nano-ZrO$_2$ composite AEMs are similar to that of
65 QCPAES membrane rather than CLQCPAES membrane. The

Table 3 Mechanical properties of QCPAES, CLQCPAES and CLQCPAES/nano-ZrO$_2$ composite membranes.

membrane	IEC (meq g^{-1})	Tensile strength (MPa)	Young's modulus (MPa)	Elongation at break (%)
QCPAES	1.25 ±0.09	21.3 ±1.3	247.0±17.6	66.7±4.6
CLQCPAES	1.06 ±0.03	25.8±2.0	346.6±20.5	33.0 ±1.2
CLQCPAES/2.5%ZrO$_2$	1.12 ±0.04	28.9 ±2.8	362.5±23.5	21.8 ±1.7
CLQCPAES/5%ZrO$_2$	1.15 ±0.06	34.4 ±2.3	352.0±26.4	25.4 ±1.4
CLQCPAES/7.5%ZrO$_2$	1.23 ±0.08	32.0 ±2.6	343.4±22.7	27.2 ±2.2
CLQCPAES/10%ZrO$_2$	1.18 ±0.06	30.4 ±3.6	492.4±32.9	20.6 ±2.3
QMPAEK-70[54]	1.22	25.56	not reported	41.08
Nafion-117[57]	0.91	21.1	6.6	370.6

zonal distribution of uniform nano-sized particles in the hydrophilic domains creates more chances for the surface hydroxyl groups of nano-particles to crosslink with the benzyl bromide groups inside the precursor hydrophilic domains. The cross-linking reaction between the hydrophobic domains and the precursor hydrophilic domains is restricted by the addtion of nano-filler. This is why the water uptakes and swelling ratios of the CLQCPAES/nano-ZrO$_2$ composite AEMs greatly depend on the filler loading and the aggeragates size of nano-filler.

3.3. Mechanical properties

The mechanical properties of the QCPAES and CLQCPAES/nano-ZrO$_2$ composite membranes were measured at room temperature and 100% RH at a stretching speed of 10 mm min^{-1}. The tensile strength, Young's modulus and elongation at break of all the membranes are listed in Table 3. Compared with QCPAES, the tensile strength and Young's modulus of the CLQCPAES membrane are enhanced enormously by the crosslinking technique and increase to 25.8 MPa and 346.6 MPa respectively. In the case of CLQCPAES/nano-ZrO$_2$ composite membranes, the tensile strength is further reinforced by the addition of nano-filler. The enhancement of mechanical properties results from the crosslinking reactions inside the polymer matrix or between the matrix and nano-filler particles, and the strong non-covalent interactions between the polymer matrix and nano-filler particles. The enhancement varies with the loadings of nano-ZrO$_2$ filler. The CLQCPAES/5%ZrO$_2$ membrane shows the optimum reinforcement and displays a maximum tensile strength up to 34.4 MPa. The reinforcement of tensile strength is weakened with the increasing filler loading at the nano-ZrO$_2$ content above 5%. The possible explanations are the enhanced plasticizing owing to higher water uptakes and the formation of nano-filler agglomerates (Fig. 5(**e**)) due to over loading. Even the effects of the plasticizing and nano-ZrO$_2$ agglomerates are negative; the positive crosslinking reaction among the hydrophilic/hydrophobic domains, crosslinking reaction and strong non-covalent interaction between the polymer matrix and the inorganic filler phase reinforce the mechanical properties of the CLQCPAES/nano-ZrO$_2$ composite AEMs at the investigating nano-ZrO$_2$ contents. Even at the maximum loading at 10%, the tensile strength and Young's modulus show 1.18 and 1.42 times to that of the CLQCPAES membrane. As to the best AEM candidate CLQCPAES/7.5%ZrO$_2$ membrane, the tensile strength is the second highest in the group of the composite membranes.

3.4. Thermal stabilities

The thermal stability is important for AEMs because AEMFCs usually work at elevated temperature. The TGA curves of CPAES, BMCPAES, QCPAES, CLQCPAES, and CLQCPAES/7.5%ZrO$_2$ are shown in Fig. 10. CPAES shows one weight loss stage behavior, which is attributed to the decomposition of main chain. The 5% weight loss temperature of CPAES is higher than 400 ^{o}C revealing the good thermal stability of CPAES. Two major weight loss stages are observed in the decomposition of BMCPAES. The first one ranging from 170 to 340 ^{o}C is assigned to the degradation of bromomethyl groups and the latter one from 410 to 610 ^{o}C is attributed to the decomposition of polymer backbone. Four weight loss stages are found at 35 to 150 ^{o}C, 150 to 230 ^{o}C, 230 to 350 ^{o}C and above 350 ^{o}C respectively in the case of QCPAES, CLQCPAES, and CLQCPAES/7.5%ZrO$_2$ membranes. They exhibit the similar degradation trends as that of the multiblock ionomer QPAE-X15Y15 derived by chloromethylation method in the previous work.[23] The degradation of quaternary ammonium groups occurs at the second weight loss stage (150 to 230 ^{o}C), which is much higher than the common working temperatures of AEMFCs (60 to 90 ^{o}C).[56] It should be pointed out that the cross-linked structure and the introduction of nano-filler have no significant effect on the thermal stability of the QCPAES based membranes.
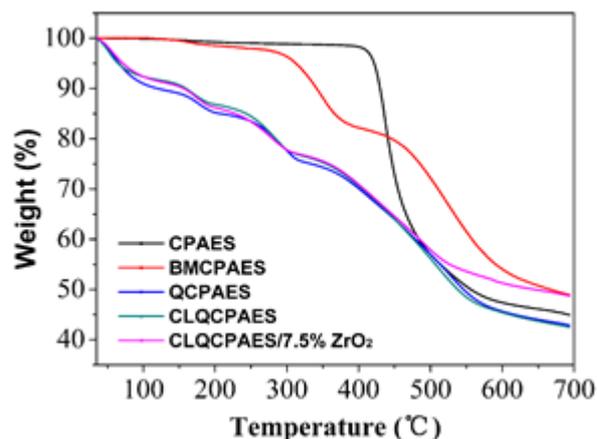
Fig. 10 TGA curves of CPAES, BMCPAES, and QCPAES, CLQCPAES, CLQCPAES/7.5%ZrO$_2$ membranes.

Table 4 Strong alkaline stability test of QCPAES, CLQCPAES and CLQCPAES/nano-ZrO$_2$ composite membranes.

membrane	concentration	Conductivity (mS cm^{-1})[a]		τ_d[b] (day)
		before	after	
QCPAES	6M NaOH	38.6	38.4	7
CLQCPAES	6M NaOH	27.4	27.3	10.5
CLQCPAES/2.5%ZrO$_2$	6M NaOH	30.8	30.9	11
CLQCPAES/5%ZrO$_2$	6M NaOH	31.1	31.1	10
CLQCPAES/7.5%ZrO$_2$	6M NaOH	42.2	42.3	11
CLQCPAES/10%ZrO$_2$	6M NaOH	38.3	38.2	12

[a] Stability test at room temperature for 48 h and measured at 60 ^{o}C.
[b] τ_d is the time at which the membranes broke into pieces at 60 ^{o}C.

Table 5 Long-term alkaline stability test of QCPAES, CLQCPAES and CLQCPAES/nano-ZrO$_2$ composite membranes.

membrane	IEC (meq g^{-1})	stability test condition	Conductivity at 60 ^{o}C (mS cm^{-1})		decreasing amplitude
			before	after	
QCPAES	1.25±0.09	1M NaOH, 60 ^{o}C, 340 h	38.4	33.8	12.0%
CLQCPAES	1.06±0.03	1M NaOH, 60 ^{o}C, 340 h	27.3	25.4	7.0%
CLQCPAES/2.5%ZrO$_2$	1.12±0.04	1M NaOH, 60 ^{o}C, 340 h	30.9	28.6	7.4%
CLQCPAES/5%ZrO$_2$	1.15±0.06	1M NaOH, 60 ^{o}C, 340 h	31.1	29.1	6.4%
CLQCPAES/7.5%ZrO$_2$	1.23±0.08	1M NaOH, 60 ^{o}C, 340 h	42.3	39.7	6.1%
CLQCPAES/10%ZrO$_2$	1.18±0.06	1M NaOH, 60 ^{o}C, 340 h	38.2	36.1	5.5%
QPAES/7.5%nano-ZrO$_2$[50]	1.74±0.03	1M NaOH, 60 ^{o}C, 170 h	30.4	not reported	9.3%
QPAES/10.0%nano-ZrO$_2$[50]	1.82±0.37	1M NaOH, 60 ^{o}C, 170 h	36.5	not reported	13.4%

3.5 Alkaline stability

The alkaline stability of AEMs is very important for their potential use in AEMFCs. The working condition of AEMs in AEMFCs is harsh alkaline environment and the working temperature ranging from 60 to 90 ^{o}C.[56] Under such conditions, the degradation occurs by two ways: the leaving of cationic groups and the decomposition of backbone. The leaving of cationic groups leads to the loss of hydroxide conductivity and the decomposition of the backbone results in a deterioration of mechanical properties. In this work we evaluated the alkaline stability of AEMs by three methods. The strong alkaline stability of membranes was explored by measuring the change in hydroxide ion conductivity after treated in 6 M NaOH at room temperature for 48 h. The results are listed in Table 4. It's clear that the strong alkaline treatments for a short time have no significant effect on conductivity of the membranes. We recorded the time（τ_d）that the AEMs broke into pieces after treated in 6 M NaOH at 60 ^{o}C (Table 4). The τ_d values of CLQCPAES and CLQCPAES/nano-ZrO$_2$ composite membranes are obviously longer than that of QCPAES membrane. The combination of crosslinking and introduction of nano-filler greatly enhanced the backbone stability. The long-term alkaline stability of the membranes was further investigated by determining the variation in hydroxide ion conductivity after treated in 1 M NaOH at 60 ^{o}C for 340 h. The results are listed in Table 5. The CLQCPAE based AEMs show obviously enhanced alkaline stability with decreasing amplitudes of conductivity less than 7.4%. The alkaline stability of CLQCPAES/nano-ZrO$_2$ composite membranes is further reinforced by the introduction of nano-filler. They give decreasing amplitudes of conductivity less than 6.4%, with the exception of CLQCPAES/2.5%ZrO$_2$. The alkaline stability of the CLQCPAES/7.5%ZrO$_2$ membrane is the second highest in the group of the composite membranes. Compared with the decreasing amplitudes of QPAES/nano-ZrO$_2$ composite membranes, which are higher than 9.3%,[50] the combination of multiblock structure and cross-linking greatly enhances the alkaline stability of CLQCPAES/nano-ZrO$_2$ composite membranes.

4. Conclusions

A series of cross-linked multiblock copoly(arylene ether sulfone) ionomer/nano-ZrO$_2$ composite anion exchange membranes are successfully fabricated by a process of controlled synthesis of multiblock precursor polymer, bromination, ultrasonication blending of solution, self-crosslinking and quaternization.

RSC Advances Accepted Manuscript

Solubility test indicates that the cross-linking network is constructed with the crosslinking points between hydrophilic domains and hydrophobic domains, and the covalent bonds forming from active surface hydroxyl groups of nano-ZrO_2 and benzyl bromide groups in the hydrophilic domains. The XRD spectra reveal that the crystallinity of composite membranes increases with the increasing content of nano-filler. SEM images display a clear zonal distribution of uniform nano-sized particles with the nano-filler loading below 7.5%. The aggregation of nano-filler is observed at a loading of 10.0%. Water uptakes and swelling ratios of the CLQCPAES/nano-ZrO_2 composite AEMs greatly depend on the filler loading and the aggregates size of nano-filler. The modification with block-ionomer structure, cross-link treatment and the introduction of nano-ZrO_2 particles greatly enhance water uptake, hydroxide conductivity, mechanical properties and alkaline stability of the composite membranes. All the CLQCPAES/nano-ZrO_2 composite membranes show hydroxide ion conductivities over 37.3 mS cm^{-1} at 80 ℃, which can satisfy the requirement of AEMs used in AEMFCs. The E_a values of the CLQCPAES/nano-ZrO_2 composite AEMs range from 17.28 to 21.26 kJ mol^{-1}. Particularly, the CLQCPAES/7.5%ZrO_2 membrane with an IEC value of 1.23 mmol g^{-1} exhibits the best comprehensive properties. It gives the highest hydroxide conductivity of 55.2 mS cm^{-1} at 80 °C, the second highest tensile strength of 32.0 MPa, and excellent alkaline stability. The membrane maintains 93.9% of its hydroxide conductivity after been treated in 1 M NaOH at 60 °C for 340 h and keeps appearance after 10 days in 6 M NaOH at 60 °C. These properties of the cross-linked hybrid membrane CLQCPAES/7.5%ZrO_2 demonstrate its potential use in AEMFCs.

Acknowledgements

Nomenclature

CLQCPAES	cross-linked multiblock copoly(arylene ether sulfone) ionomer
QCPAES	multiblock copoly(arylene ether sulfone) ionomer
QPAES	random poly(arylene ether sulfone) ionomer
AEMFCs	alkaline anion exchange membrane fuel cells
IEC	ion-exchange capacity
AEM	Anion exchange membrane
XRD	X-ray diffraction
SEM	scanning electron microscopy
TGA	thermogravimetric analysis
FPS	Bis(4-fluorophenyl) sulfone
nano-ZrO_2	Nano-zirconia filler
TMBP	3,3',5,5'-tetramethyl-4,4'-dihydroxybiphenyl
HPDPM	Bis(4-hydroxylphenyl)diphenylmethane
NBS	N-bromosuccinimide
AIBN	azodiisobutyronitrile
DMAc	N-dimethylacetamide
DMF	N,N-dimethylformamide
BMCPAES	bromomethylated multiblock copoly(arylene ether sulfone)
WU	water uptake
SR	swelling ratio
E_a	ion transport activation energy

References

1. L. Carrette, K. A. Friedrich and U. Stimming, *Fuel Cells*, 2001, **1**, 5-39.
2. M. A. Hickner, H. Ghassemi, Y. S. Kim, B. R. Einsla and J. E. McGrath, *Chem. Rev.*, 2004, **104**, 4587-4612.
3. M. Winter and R. J. Brodd, *Chem. Rev.*, 2004, **104**, 4245-4270.
4. M. S. Whittingham and T. Zawodzinski, *Chem. Rev.*, 2004, **104**, 4243-4244.
5. J. R. Varcoe, R. C. T. Slade and E. Lam How Yee, *Chem. Commun.*, 2006, 1428-1429.
6. J. Fang and P. K. Shen, *J. Membr. Sci.*, 2006, **285**, 317-322.
7. J. R. Varcoe and R. C. T. Slade, *Fuel Cells*, 2005, **5**, 187-200.
8. L. Jörissen, V. Gogel, J. Kerres and J. Garche, *J. Power Sources,* 2002, **105**, 267-273.
9. K. Matsuoka, Y. Iriyama, T. Abe, M. Matsuoka and Z. Ogumi, *J. Power Sources*, 2005, **150**, 27-31.
10. N. Fujiwara, Z. Siroma, S.-i. Yamazaki, T. Ioroi, H. Senoh and K. Yasuda, *J. Power Sources*, 2008, **185**, 621-626.
11. C. Coutanceau, L. Demarconnay, C. Lamy and J. M. Léger, *J. Power Sources*, 2006, **156**, 14-19.
12. J. R. Varcoe, R. C. T. Slade, E. L. H. Yee, S. D. Poynton and D. J. Driscoll, *J. Power Sources*, 2007, **173**, 194-199.
13. S. Lu, J. Pan, A. Huang, L. Zhuang and J. Lu, *Proc. Natl. Acad. Sci. U.S.A.*, 2008, **105**, 20611-20614.
14. Y. S. Li and T. S. Zhao, *Int. J. Hydrogen Energy*, 2012, **37**, 4413-4421.
15. X. Li, Y. Yu, Q. Liu and Y. Meng, *ACS Appl. Mater. Interfaces*, 2012, **4**, 3627-3635.
16. X. Li, Q. Liu, Y. Yu and Y. Meng, *J. Mater. Chem. A*, 2013, **1**, 4324-4335.
17. X. Yan, G. He, S. Gu, X. Wu, L. Du and H. Zhang, *J. Membr. Sci.*, 2011, **375**, 204-211.
18. J. Yan and M. A. Hickner, *Macromolecules*, 2010, **43**, 2349-2356.
19. Z. Zhao, J. Wang, S. Li and S. Zhang, *J. Power Sources*, 2011, **196**, 4445-4450.
20. S. Xu, G. Zhang, Y. Zhang, C. Zhao, L. Zhang, M. Li, J. Wang, N. Zhang and H. Na, *J. Mater. Chem.*, 2012, **22**, 13295-13302.
21. S. Xu, G. Zhang, Y. Zhang, C. Zhao, W. Ma, H. Sun, N. Zhang, L. Zhang, H. Jiang and H. Na, *J. Power Sources*, 2012, **209**, 228-235.
22. M. Tanaka, K. Fukasawa, E. Nishino, S. Yamaguchi, K. Yamada, H. Tanaka, B. Bae, K. Miyatake and M. Watanabe, *J. Am. Chem. Soc.*, 2011, **133**, 10646-10654.
23. X. Li, Y. Yu, Q. Liu and Y. Meng, *J. Membr. Sci.*, 2013, **436**, 202-212.
24. D. Chen, M. A. Hickner, E. Agar and E. C. Kumbur, *Electrochem. Commun.*, 2013, **26**, 37-40.
25. G. Liu, Y. Shang, X. Xie, S. Wang, J. Wang, Y. Wang and Z. Mao, *Int. J. Hydrogen Energy*, 2012, **37**, 848-853.
26. J. Zhou, M. Ünlü, I. Anestis-Richard, H. Kim and P. A. Kohl, *J. Power Sources*, 2011, **196**, 7924-7930.
27. H. Hou, G. Sun, R. He, B. Sun, W. Jin, H. Liu and Q. Xin, *Int. J. Hydrogen Energy*, 2008, **33**, 7172-7176.
28. G. Wang, Y. Weng, D. Chu, D. Xie and R. Chen, *J. Membr. Sci.*, 2009, **326**, 4-8.
29. X. Lin, X. Liang, S. D. Poynton, J. R. Varcoe, A. L. Ong, J. Ran, Y. Li, Q. Li and T. Xu, *J. Membr. Sci.*, 2013, **443**, 193-200.
30. J. Zhang, T. Zhou, J. Qiao, Y. Liu and J. Zhang, *Electrochim. Acta*, 2013, **111**, 351-358.
31. W. Lu, Z.-G. Shao, G. Zhang, Y. Zhao and B. Yi, *J. Power Sources*, 2014, **248**, 905-914.
32. A. H. N. Rao, R. L. Thankamony, H.J. Kim, S. Nam and T.H. Kim, *Polymer*, 2013, **54**, 111-119.
33. N. T. Rebeck, Y. Li and D. M. Knauss, *J. Polym. Sci., Part B: Polym. Phys.*, 2013, **51**, 1770-1778.

RSC Advances Accepted Manuscript

34. Z. Liu, X. Zhu, G. Wang, X. Hou and D. Liu, *J. Polym. Sci., Part B: Polym. Phys.*, 2013, **51**, 1632-1638.

35. N. J. Robertson, H. A. Kostalik, T. J. Clark, P. F. Mutolo, H. D. Abruña and G. W. Coates, *J. Am. Chem. Soc.*, 2010, **132**, 3400-3404.

5   36. J. Wang, G. He, X. Wu, X. Yan, Y. Zhang, Y. Wang and L. Du, *J. Membr. Sci.*, 2014, **459**, 86-95.

37. J. Zhang, J. Qiao, G. Jiang, L. Liu and Y. Liu, *J. Power Sources*, 2013, **240**, 359-367.

38. L. Wu and T. Xu, *J. Membr. Sci.*, 2008, **322**, 286-292.

10   39. J. Ni, C. Zhao, G. Zhang, Y. Zhang, J. Wang, W. Ma, Z. Liu and H. Na, *Chem. Commun.*, 2011, **47**, 8943-8945.

40. R. K. Nagarale, W. Shin and P. K. Singh, *Polym. Chem.*, 2010, **1**, 388-408.

41. A. A. Mohamad and A. K. Arof, *Mater. Lett.*, 2007, **61**, 3096-3099.

15   42. Y. Wu, J. Luo, L. Yao, C. Wu, F. Mao and T. Xu, *J. Membr. Sci.*, 2012, **399–400**, 16-27.

43. Y. Wu, J. Hao, C. Wu, F. Mao and T. Xu, *J. Membr. Sci.*, 2012, **423–424**, 383-391.

44. C.C. Yang, S.-S. Chiu, S.C. Kuo and T.H. Liou, *J. Power Sources*, 20   2012, **199**, 37-45.

45. S. Sang, J. Zhang, Q. Wu and Y. Liao, *Electrochim. Acta*, 2007, **52**, 7315-7321.

46. L. Zeng, T. S. Zhao and Y. S. Li, *Int. J. Hydrogen Energy*, 2012, **37**, 18425-18432.

25   47. C.C. Yang, W.-C. Chien and Y. J. Li, *J. Power Sources*, 2010, **195**, 3407-3415.

48. C.C. Yang, *J. Membr. Sci.*, 2007, **288**, 51-60.

49. P. T. Nonjola, M. K. Mathe and R. M. Modibedi, *Int. J. Hydrogen Energy*, 2013, **38**, 5115-5121.

30   50. X. Li, Y. Yu and Y. Meng, *ACS Appl. Mater. Interfaces*, 2013, **5**, 1414-1422.

51. R. Vinodh, M. Purushothaman and D. Sangeetha, *Int. J. Hydrogen Energy* 2011, **36**, 7291-7302.

52. J. Yan, H. D. Moore, M. R. Hibbs and M. A. Hickner, *J. Polym. Sci., 35   Part B: Polym. Phys.*, 2013, **51**, 1790-1798.

53. M. R. Hibbs, C. H. Fujimoto and C. J. Cornelius, *Macromolecules*, 2009, **42**, 8316-8321.

54. K. Z. Shen, J. H. Pang, S. N. Feng, Y. Wang and Z. H. Jiang, *J. Membr. Sci.*, 2013, **440**, 20-28.

40   55. L. Wang, Y. Z. Meng, S. J. Wang, X. Y. Shang, L. Li and A. S. Hay, *Macromolecules*, 2004, **37**, 3151-3158.

56. G. Merle, M. Wessling and K. Nijmeijer, *J. Membr. Sci.*, 2011, **377**, 1-35.

57. B. Lin, L. Qiu, B. Qiu, Y. Peng and F. Yan, *Macromolecules*, 2011, 45   **44**, 9642-9649.